Research article

NMR IN BIOMEDICINE

Received: 9 June 2014, Revised: 4 September 2014, Accepted: 10 September 2014, Published online in Wiley Online Library

(wileyonlinelibrary.com) DOI: 10.1002/nbm.3225

Accelerated three-dimensional cine phase contrast imaging using randomly undersampled echo planar imaging with compressed sensing reconstruction

Tamer A. Basha, Mehmet Akçakaya, Beth Goddu, Sophie Berg and Reza Nezafat*

The aim of this study was to implement and evaluate an accelerated three-dimensional (3D) cine phase contrast MRI sequence by combining a randomly sampled 3D *k*-space acquisition sequence with an echo planar imaging (EPI) readout. An accelerated 3D cine phase contrast MRI sequence was implemented by combining EPI readout with randomly undersampled 3D *k*-space data suitable for compressed sensing (CS) reconstruction. The undersampled data were then reconstructed using low-dimensional structural self-learning and thresholding (LOST). 3D phase contrast MRI was acquired in 11 healthy adults using an overall acceleration of 7 (EPI factor of 3 and CS rate of 3). For comparison, a single two-dimensional (2D) cine phase contrast scan was also performed with sensitivity encoding (SENSE) rate 2 and approximately at the level of the pulmonary artery bifurcation. The stroke volume and mean velocity in both the ascending and descending aorta were measured and compared between two sequences using Bland–Altman plots. An average scan time of 3 min and 30 s, corresponding to an acceleration rate of 7, was achieved for 3D cine phase contrast scan with one direction flow encoding, voxel size of $2 \times 2 \times 3$ mm^3, foot–head coverage of 6 cm and temporal resolution of 30 ms. The mean velocity and stroke volume in both the ascending and descending aorta were statistically equivalent between the proposed 3D sequence and the standard 2D cine phase contrast sequence. The combination of EPI with a randomly undersampled 3D *k*-space sampling sequence using LOST reconstruction allows a seven-fold reduction in scan time of 3D cine phase contrast MRI without compromising blood flow quantification. Copyright © 2014 John Wiley & Sons, Ltd.

Keywords: phase contrast MR; 4D flow; compressed sensing; echo planar imaging

INTRODUCTION

Phase contrast MRI allows the measurement of the blood flow velocity in the heart and the great vessels (1,2). Two-dimensional (2D) cine phase contrast is widely used clinically for time-resolved quantification of blood flow through the great vessels. Recent advances in fast imaging and respiratory motion correction have enabled imaging of three-dimensional (3D) time-resolved phase contrast for comprehensive evaluation of three-dimensionally and three directionally encoded blood velocity (3–5). This sequence has been used widely to study the blood flow hemodynamics associated with cardiac and vascular diseases (6–14).

Despite the potential of 3D cine phase contrast imaging in the comprehensive evaluation of blood hemodynamics, it has a long scan time which typically exceeds 10 min. Therefore, it is not clinically feasible to acquire four-dimensional (4D) cine phase contrast as part of a comprehensive cardiac MRI protocol, which commonly includes the evaluation of function, anatomy, perfusion and scar imaging. Furthermore, longer scan times are more susceptible to heart rate variations and respiratory motion that could hinder the measurement accuracy and reproducibility.

Over the past decade, several acceleration techniques have been used to reduce the scan time of cine phase contrast sequences. Parallel imaging is widely accepted as the most robust and accessible technique to reduce the scan time by two- to three-fold (15–17). Non-Cartesian trajectories, including both radial (18,19) and spiral (20,21), have also been used to reduce the scan time. Higher acceleration rates (>3) have been achieved using methods that exploit the spatiotemporal correlations, such as *k–t* sensitivity encoding (SENSE), *k–t* broad-use linear acquisition speed-up technique (BLAST) (22,23), *k–t* generalized autocalibrating partially parallel acquisition (GRAPPA)

* *Correspondence to: R. Nezafat, Beth Israel Deaconess Medical Center, 330 Brookline Ave., Boston, MA 02215, USA.*
E-mail: rnezafat@bidmc.harvard.edu

T. A. Basha, M. Akçakaya, B. Goddu, S. Berg, R. Nezafat
Department of Medicine (Cardiovascular Division), Beth Israel Deaconess Medical Center and Harvard Medical School, Boston, MA, USA

Abbreviations used: *BLAST, broad-use linear acquisition speed-up technique; CS, compressed sensing; 2D/3D/4D, two/three/four-dimensional; ECG, electrocardiogram; EPI–CS, echo planar imaging with compressed sensing; FFT, fast Fourier transform; FOV, field of view; GRAPPA, generalized autocalibrating partially parallel acquisition; LOST, low-dimensional structural self-learning and thresholding; NAV, navigator; PCA, principal component analysis; RF, radiofrequency; ROI, region of interest; SENSE, sensitivity encoding; SSFP, steady-state free precession; LGE, late gadolinium enhancement.*

Copyright © 2014 John Wiley & Sons, Ltd.

(24,25) and *k–t* principal component analysis (PCA) (26,27). Although *k–t* approaches have been shown to surpass the acceleration rates achievable by parallel imaging, they may suffer from temporal blurring as a result of intrinsic temporal filtering, which may influence the accuracy of the peak velocity measurement. Using acceleration factors on the order of 8 or more has been shown to introduce discrepancies in the measured velocities (22), and a six-fold *k–t* BLAST sequence has exhibited a reduction in peak velocity relative to SENSE with acceleration rate 2 (23).

Compressed sensing (CS) has been used recently to accelerate 2D and 3D cine phase contrast imaging (28,29). Several methods have been proposed for phase reconstruction from undersampled phase contrast data using different sparsity-promoting approaches (30,31). A combination of spatiotemporal (*k–t*)-based CS and parallel imaging, called *k–t* SPARSE-SENSE, has also been used to reduce the scan time, which showed good agreement with the results from GRAPPA (32). Moreover, aliasing artifacts caused by static tissues, resulting from CS reconstruction, have been shown not to affect flow quantification, as these may be canceled out during the phase subtraction process (33). Several *in vivo* studies have validated the results of flow imaging with CS relative to established parallel imaging acceleration techniques (34–36).

An alternative established way to reduce the scan time is to use echo planar imaging (EPI) readout, in which multiple *k*-space lines are acquired after each radiofrequency (RF) excitation. This is particularly useful for phase contrast imaging, where bipolar gradients are applied after each RF excitation, which elongates TR and thus the scan time. Single-shot and multi-shot EPI were used early on to accelerate 2D phase contrast imaging (37–39). The effect of flow and motion sensitivity on flow measurements using EPI acquisition has been studied extensively (40–42), and several methods have been proposed to reduce these effects (43,44). Recent advances in the hardware components of the MR system and reconstruction techniques have allowed EPI to be used for faster phase contrast imaging with higher temporal and spatial resolution (45,46).

In this study, we sought to investigate the feasibility of an accelerated 3D cine phase contrast sequence which combines the efficient data sampling strategy of EPI with a randomly undersampled 3D *k*-space sampling pattern followed by with a CS reconstruction. In a pilot study, we evaluated different combinations of acceleration factors using CS and EPI to accelerate 3D phase contrast MRI. Subsequently, we compared the flow measurements from a seven-fold-accelerated 3D cine phase contrast MRI acquisition using the proposed combination of CS and EPI with those from a conventional two-fold-accelerated 2D cine phase contrast MRI acquisition.

MATERIALS AND METHODS

The imaging protocol was approved by our institutional review board. Written informed consent was obtained from all participants. All patients were scanned using a 1.5-T Philips Achieva scanner (Philips Healthcare, Best, the Netherlands) with a 32-channel cardiac phased array receiver coil.

Pulse sequence

Figure 1 shows the proposed 3D EPI–CS cine phase contrast imaging sequence. Figure 1a shows the standard interleaved flow sequence with flow encoding in only one direction. Thus, for each time frame, two flow encodings are played, each followed by an acquisition. Figure 1b shows a schematic diagram for one of these encoding/acquisition pairs. Directly after the flow encoding gradients, an EPI strategy is used to sample multiple lines of *k* space instead of one single line. This leads to a longer TR, but allows flow gradients to be played only once for multiple *k*-space lines.

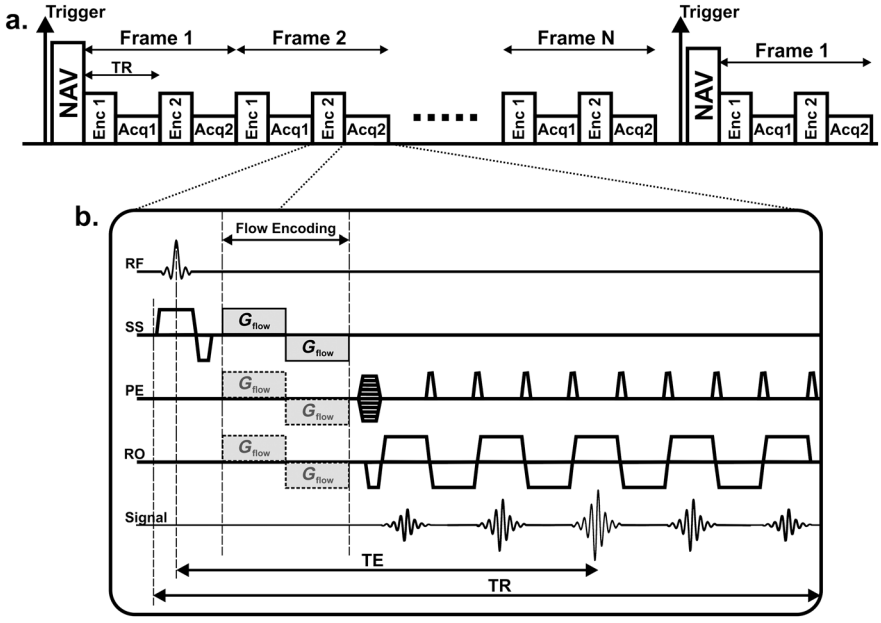

Figure 1. Pulse sequence diagram for the cine phase contrast sequence with an echo planar imaging (EPI) readout and compressed sensing (CS) undersampling. (a) A diagram for the standard interleaved flow sequence with flow encoded in only one direction. (b) Following the flow encoding gradient, an EPI readout is used to acquire multiple lines of *k* space.

Copyright © 2014 John Wiley & Sons, Ltd.

NMR IN BIOMEDICINE

k Space and acceleration

To accelerate the scan time using the CS technique, the *k*-space profiles are randomly undersampled, such that only a fraction of the profiles is acquired. Figure 2a shows k_y–k_z maps for a conventional randomly undersampled *k* space of a 3D acquisition with an acceleration rate of 3. To combine this with an EPI acquisition, the *k* space is divided into multiple segments, where each segment is an exact replica of the others. Figure 2b shows an example k_y–k_z map divided into three similar segments for an EPI rate of 3. Each segment is randomly undersampled, such that the overall CS acceleration rate remains the same (3 in this example). During acquisition, for each point picked from the first segment, the gradient blips are used to jump in *k* space to the corresponding points in the other EPI segments.

It is usually advantageous for CS reconstruction to fully sample the *k*-space center area as shown by the white rectangle in Fig. 2a. However, as a result of the EPI acquisition pattern, this area needs to be exactly replicated into each single EPI segment (white rectangles in Fig. 2b). Thus, although the fully sampled area in the center segment is necessary for the CS reconstruction (being the center of *k* space), the center areas of the side segments are not necessarily required to be fully sampled, but rather result from the EPI acquisition pattern.

Profile ordering

Profile ordering determines when each *k*-space line is acquired during the acquisition. In a multi-shot acquisition, an arbitrary profile ordering for a randomly undersampled *k* space results in non-uniform jumps in *k* space, which is associated with large gradient switching, resulting in eddy current artifacts, especially with a steady-state free precession (SSFP) sequence. In order to reduce this effect, a special radial profile ordering was proposed in refs. (47,48). In this work, we combined this radial ordering with the EPI acquisition strategy, as shown in Fig. 3. Starting from a regular linear ordering (Fig. 3a), the EPI method divides the *k*-space profiles into R_{EPI} segments, based on the EPI factor; then, one *k*-space line of each segment (i.e. R_{EPI} lines) is acquired for the same RF excitation (Fig. 3b). This leads to an approximate reduction rate of R_{EPI}. However, the proposed CS acquisition is based on a radial profile ordering (Fig. 3c), whilst randomly undersampling the profiles by a factor of R_{CS} and keeping the *k*-space center fully sampled (Fig. 3d). This results in a reduction rate of exactly R_{CS}. Then, to combine both methods, we apply the radial ordering mechanism to each EPI segment, as shown in Fig. 3e. This leads to an approximate reduction rate of $R_{EPI} \times R_{CS}$. The actual reduction rate of the scan time is lower because of the longer TR when EPI is used. Thus, keeping the same phase interval, the actual acceleration rate is slightly lower than the theoretical rate of $R_{EPI} \times R_{CS}$.

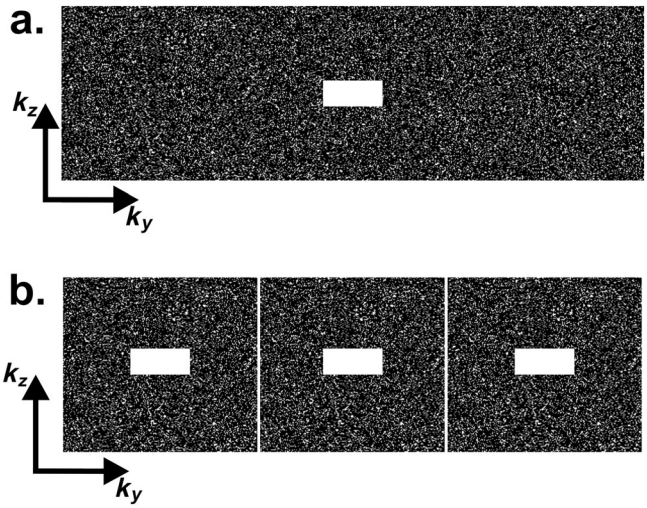

Figure 2. (a) k_y–k_z map for the regular randomly undersampled *k* space, whilst keeping the center lines fully sampled (≈10–15% in k_y and k_z). Each dot in the map represents a line in *k* space (i.e. one readout profile). The white dots represent the acquired lines and the black dots represent the non-acquired lines. (b) The *k*-space undersampling is adapted to an echo planar imaging (EPI) acquisition of rate 3. The *k* space is divided into three similar blocks. Then, during acquisition, each EPI shot consists of one line from each block.

3D EPI–CS scan protocol

In all the subsequent *in vivo* scans, the following protocol was used. Scout images were acquired with an SSFP sequence with an in-plane resolution of $3 \times 3\,mm^2$ and a slice thickness of 10 mm, which was used for localization and assignment of the appropriate imaging slab covering the ascending and descending aorta, and the pulmonary bifurcation. A free-breathing electrocardiogram (ECG)-triggered gradient echo sequence was used for acquisition. The trigger delay was chosen to be 20 ms following the acquisition of the leading navigator (NAV) signal. Arrhythmia rejection was utilized, allowing the sampling of up to 90% of the cardiac cycle. A NAV placed on the dome of the right hemidiaphragm with a duration of 17 ms was used for respiratory motion measurement, utilizing prospective real-time correction and a superior–inferior tracking ratio of 0.6 (49,50). For the EPI–CS cine phase contrast sequence, images were acquired axially using a 3D gradient echo with an EPI–CS acceleration [field of view (FOV), $340 \times 280 \times 60\,mm^3$; resolution, $2 \times 2 \times 3\,mm^3$; turbo factor, i.e. number of excitations per cardiac phase, 2; TR/TE/α = 4.7 ms/2.3 ms/10°] in a volume covering the ascending and descending aorta at the level of the pulmonary artery bifurcation. Only one flow encoding, in the foot–head direction, with velocity encoding of 400 cm/s, was used, which provides an adequate temporal resolution of 30 ms for the output cine images. Several EPI and CS rates (i.e. R_{EPI}, R_{CS}) were used during the study, as described in the following subsections.

Selection of the acceleration rate parameters

In order to investigate the impact of different CS acceleration rates and EPI factors on image quality, we performed a pilot study in 13 healthy adults (32 ± 15 years; three men). Images were acquired using the 3D EPI–CS cine phase contrast sequence employing different combinations of EPI factors and CS rates. We investigated various EPI factors of 3, 5, 7 and 9 with CS acceleration rates of 3, 4 and 5. TR/TE/α = 7.4 ms/3.8 ms/10°, TR/TE/α = 9.0 ms/4.7 ms/10°, TR/TE/α = 11 ms/5.7 ms/20° and TR/TE/α = 13 ms/6.7 ms/20° for EPI rates of 3, 5, 7 and 9, respectively. We note that not all possible combinations of these two parameters were performed because of the limited scan time. Flow images were visually inspected for artifacts, temporal smoothing and inhomogeneity artifacts commonly associated with high EPI rates, and aliasing artifacts commonly associated with high CS

Copyright © 2014 John Wiley & Sons, Ltd.

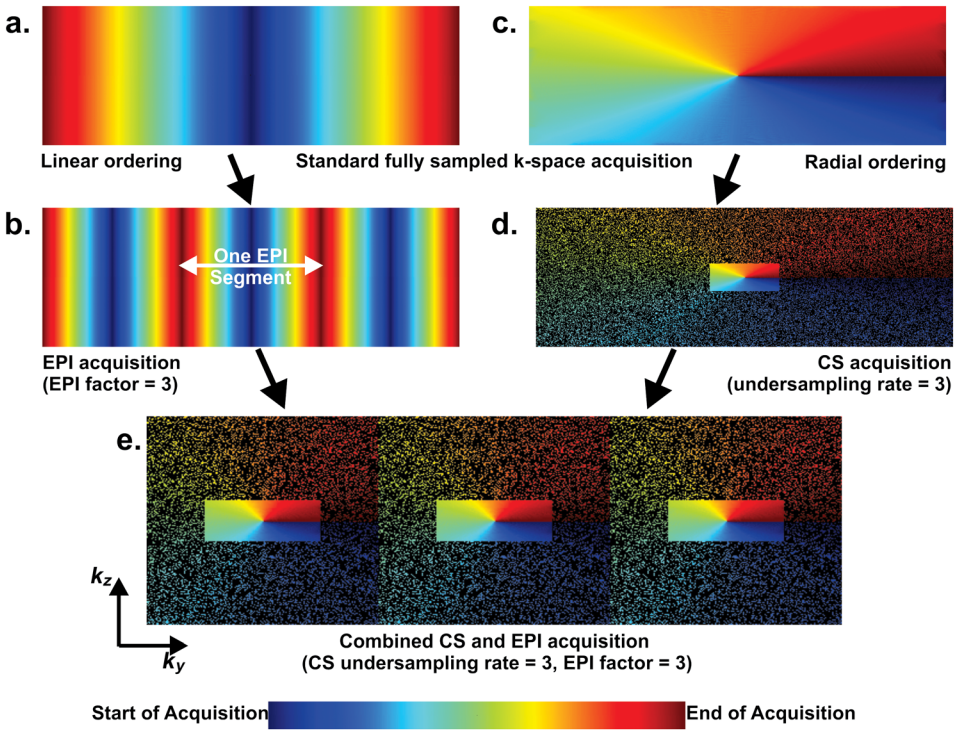

Figure 3. *k*-space acquisition strategy: with conventional three-dimensional (3D) imaging, the profiles are spanned/acquired in either a linear (a) or radial (c) ordering fashion in the k_y–k_z plane. Based on the linear ordering strategy, echo planar imaging (EPI) acceleration (b) divides *k* space into multiple segments, where one line from each segment is acquired within the same EPI shot. In contrast, compressed sensing (CS) acceleration (d) is primarily based on radial ordering, where the *k*-space profiles are randomly undersampled and acquired in a radial fashion, whilst keeping the center area of *k* space fully sampled. Both EPI and CS can be combined into one acquisition with a higher acceleration rate, as shown in (e). Although *k* space is divided into multiple segments, each segment is randomly undersampled with the same pattern and then acquired in a radial fashion. The major advantage is the high overall acceleration rate (9 in this example) for the whole 3D acquisition, whereas one drawback is the need to fully sample parts of *k* space even if they are not at the center of *k* space.

rates. Any other artifacts that might affect the flow quantification as a result of the combination of EPI and CS were also noted.

3D EPI–CS *versus* 2D cine phase contrast

Eleven healthy adults (29 ± 12 years; five men) underwent 3D EPI–CS cine phase contrast. For each subject, the 3D EPI–CS cine phase contrast scan was followed by a standard breath-hold 2D cine phase contrast scan with the same flow encoding direction with the following parameters: FOV, $340 \times 280\ mm^2$; resolution, $2 \times 2\ mm^2$; slice thickness, 5 mm; TR/TE/α = 4.7 ms/2.3 ms/10°; SENSE rate of 2. The 2D slice was selected using the 3D scan, approximately at the pulmonary artery bifurcation.

In addition, in a subset of five subjects, a 4D phase contrast scan was performed as a reference. In this reference scan, the same FOV, TR/TE, spatial and temporal resolutions were prescribed, but a uniform undersampling rate of 4 (2×2 in k_y and k_z, respectively), together with the commercially available SENSE reconstruction, was utilized.

Image reconstruction

The raw *k*-space data of the EPI–CS cine phase contrast scans were exported to perform off-line CS reconstruction, using the low-dimensional structural self-learning and thresholding (LOST) method (47) for the estimation of the missing *k*-space lines for the randomly undersampled datasets. A B_1-weighted version of this algorithm was employed to utilize the coil sensitivity information (51). In LOST, an image estimate is used to adaptively identify 2D image blocks of similar signal content, which are grouped into similarity clusters. This is performed by block matching within a search neighborhood for each voxel of the image, where the $N_b \times N_b$ reference block, whose top left corner is at that voxel, is compared using the normalized l_2 distance to another block, which are declared to be similar if this distance is less than a threshold λ_{match}, and the compared block is added to the similarity cluster of that voxel. Subsequently, a 3D fast Fourier transform (FFT) is applied to each similarity cluster to adaptively sparsify the data (47). Aliasing is removed by thresholding the 3D FFT coefficients of the similarity clusters. For the B_1-weighted iterative reconstruction (51), the coil sensitivity maps were generated from the fully sampled central *k*-space using Hanning filtering in the k_y–k_z direction. LOST reconstruction was implemented in Matlab (v7.6, The MathWorks, Natick, MA, USA), with the adaptive learning and nonlinear shrinkage portions implemented in C++. The parameters for LOST were chosen on the basis of our previous experience with its application in LGE (47,52) and coronary imaging (51,53) as follows: $N_b = 4$, $\lambda_{match} = 0.05$ and a search neighborhood of radius 6 in the *x*–*y* direction and radius 1 in the *z* direction. The maximum number of blocks in a similarity cluster was limited to eight. For de-aliasing, LOST alternated between hard thresholding and Wiener filtering, with thresholding parameters τ_{ht} and τ_{wie}, respectively, set to 0.015 and 0.02 times the largest coefficient of the estimate from the first stage. The same reconstruction parameters were used in all cases, allowing for fully

Copyright © 2014 John Wiley & Sons, Ltd.

NMR IN BIOMEDICINE

automated reconstructions. The whole reconstruction process required an average time of 1 h per one 3D flow dataset on our institution CPU cluster.

Image and statistical analysis

All images were exported into a separate PC station for quantitative analysis to evaluate the proposed pulse sequence. For each subject, two acquisitions were evaluated: (i) the breath-hold 2D flow acquisition; and (ii) the proposed undersampled 3D cine phase contrast after reconstruction. First, given the 2D scan, the closest matching slice in the 3D volume was visually selected. Second, for each slice, a region of interest (ROI) was manually drawn on the ascending and descending aorta across different time frames (i.e. cardiac phases) using the magnitude images in each set. The ROIs were manually corrected throughout the cardiac cycle for cardiac motion. The stroke volume and mean velocity curve for the blood flow were calculated for each acquisition.

All statistical analyses were performed using Matlab (v7.14, The MathWorks) and SPSS (v20.0, SPSS Inc., Chicago, IL, USA). To assess the similarity of the measurements, a linear model analysis was used for all measurement parameters, including stroke volume and mean velocities in the ascending and descending aorta. In order to capture the measurement variability within and between subjects, the data from the 2D sequence for all subjects were structured into one single vector with an indicator variable for time within subject. The data from the 3D EPI–CS cine phase contrast sequence were structured in the same way. The overall slope between these two vectors, as well as the 95% confidence intervals, was computed taking into account the correlation of the measurements within each subject. The measurements were considered to be equivalent if the confidence interval covered 1.0. The correlation (variance–covariance) structure was assumed to be compound symmetry, which yielded the within- and between-subject variance components used in the estimation of the difference and confidence interval via a linear mixed-effects model. Bland–Altman analyses were performed to compare the stroke volume values between the 2D scans and the corresponding slices in the 3D EPI–CS cine phase contrast scans.

RESULTS

EPI and CS acceleration parameter selection

Figure 4a shows the flow images from one subject in the pilot study, each with different EPI factors (3,5,7,9). Although a higher EPI factor results in a lower scan time, higher imaging artifacts and lower signal-to-noise ratio are observed. Phase and inhomogeneity artifacts are noticeable with factors higher than 5 (yellow single-headed arrows). Furthermore, temporal smoothing occurs with higher TRs associated with the higher EPI factors (blue double-headed arrows). Figure 4b shows the flow image results when using different combinations of EPI factors (3,5) and CS rates (2–4). A similar image quality in terms of flow artifacts is seen for all rates, where the image compression-type blurring artifacts increase with increasing acceleration rate.

3D EPI–CS *versus* 2D cine phase contrast

The average scan time for the 3D EPI–CS cine phase contrast scan was 3 min and 30 s, assuming 100% NAV gating efficiency and with a phase interval of 30 ms. Without any acceleration, the nominal scan time for imaging with similar spatial and temporal resolution is approximately 31 min and 25 s, with a phase

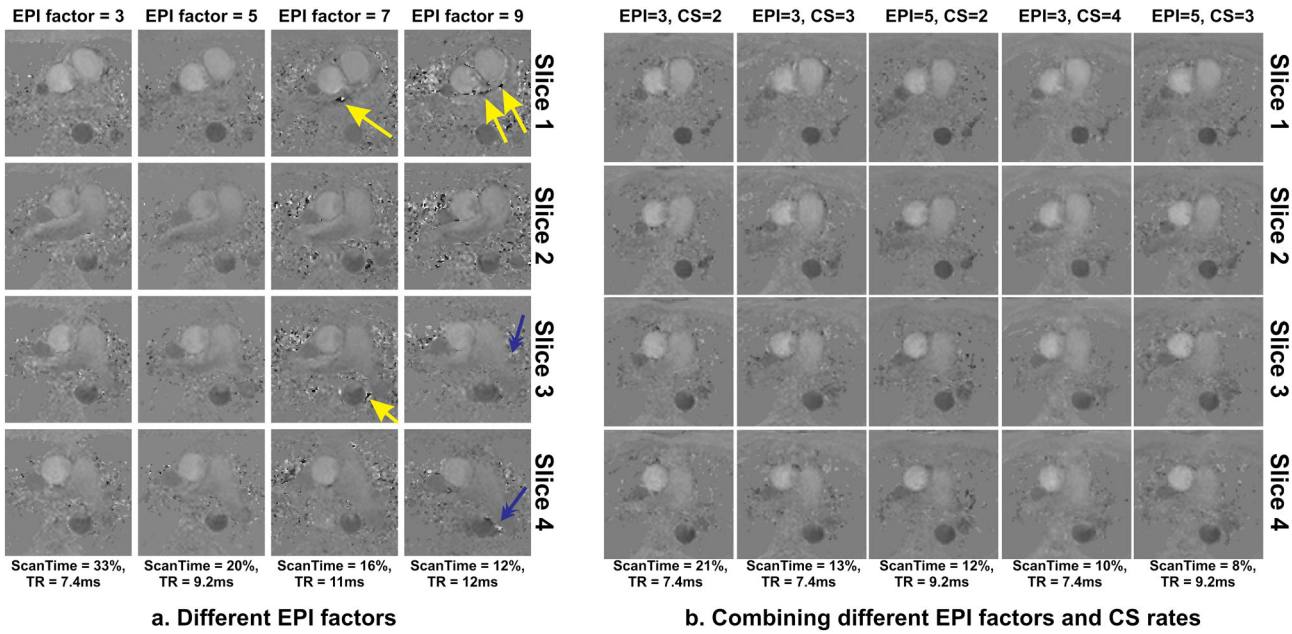

Figure 4. (a) Example flow images for four different acquisitions using echo planar imaging (EPI) factors of 3, 5, 7 and 9. Each column represents a separate scan with different EPI factor, and each row represents a specific slice at the same time frame from the three-dimensional (3D) acquisitions. Slices and time frames are visually chosen to have approximately the same location in 3D, and the same phase of the cardiac cycle. We note that images acquired with EPI factors of 3 and 5 show reasonable image quality. However, field inhomogeneity and temporal smoothing artifacts show up clearly for higher EPI factors (i.e. 7 and 9). (b) Example phase contrast images acquired using EPI factors of 3 and 5 with compressed sensing (CS) rates of 2, 3 and 4, leading to different acceleration rates.

Copyright © 2014 John Wiley & Sons, Ltd.

interval of 24.5 ms, which corresponds to an approximate reduction of the scan time by a factor of seven for the same phase interval (i.e. temporal resolution). When using SENSE as a standard parallel imaging technique, the scan time reduces to 8 min and 40 s (with an overall SENSE rate of 4, two in each phase encoding direction, i.e. k_y and k_z).

Figure 5 shows example flow images at different slices and different time frames from one representative subject using

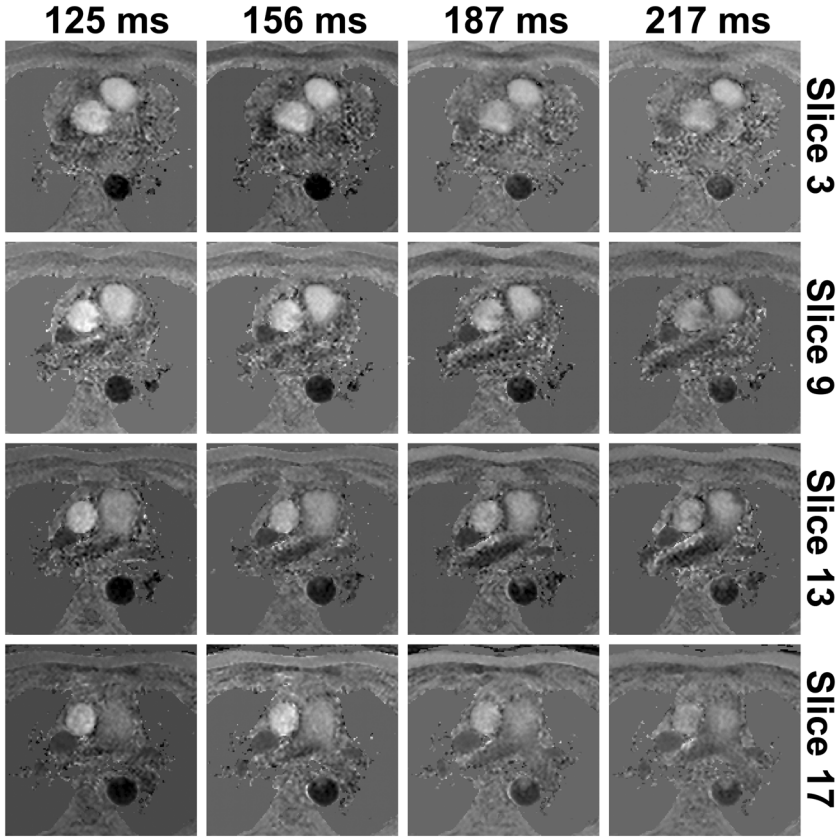

Figure 5. Example flow images for various slices and cardiac phases (specified by time after the R wave) of three-dimensional (3D) cine phase contrast MRI acquisitions from a subject with a heart rate of 75 beats/min, acquired using the proposed echo planar imaging–compressed sensing (EPI–CS) sequence, depicting cross-sections across the descending aorta and ascending aorta. The flow patterns through the ascending and descending aorta are shown, and are not hindered by the relatively high acceleration rate applied during the scan (≈7).

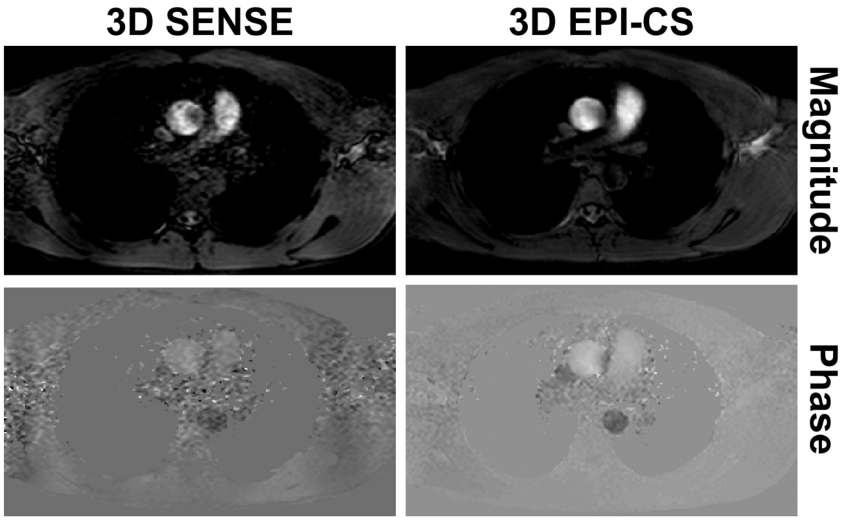

Figure 6. Representative magnitude and flow images from three dimensional sensitivity encoding (3D SENSE) and 3D echo planar imaging–compressed sensing (EPI–CS) cine phase contrast scans. The flow images in 3D SENSE show a higher level of noise and signal loss relative to those in 3D EPI–CS.

Copyright © 2014 John Wiley & Sons, Ltd.

NMR IN BIOMEDICINE

the proposed 3D EPI–CS cine phase contrast sequence. It should be noted that, although the signal-to-noise ratio is inherently low, the phase information and structure are well preserved in the 3D acquisition despite the high acceleration rate (EPI factor of 3, CS rate of 3, overall acceleration of approximately 7 for the same temporal resolution).

Figure 6 shows the magnitude and flow images acquired using uniform undersampling (acceleration rate, 2×2) with SENSE reconstruction, with a scan time of 8 min and 20 s, and the proposed 4D EPI–CS sequence with a scan time of 3 min and 24 s, assuming 100% NAV efficiency in both scans. Despite having a longer scan time, the magnitude and flow image of the SENSE-accelerated data are of lower image quality which is not sufficient for clinical usage.

Figure 7 shows the magnitude and flow images from the standard 2D flow acquisition, and the matching slice from the 3D volume result of the proposed 3D EPI–CS sequence. The image quality is clearly better in the 2D acquisition, especially in the anatomical images. However, the flow information in 3D EPI–CS is well preserved through the time frames, and visually matches that in the corresponding 2D flow images.

Figure 8a shows an example flow curve of the mean velocity of the blood flow through the ascending aorta from 2D and 3D EPI–CS cine phase contrast. The overall flow curve and peaks are comparable between the two acquisitions. Figure 8b shows the Bland–Altman plot for the stroke volume between 3D CS-EPI and 2D cine phase contrast in both the ascending and descending aorta in all 11 subjects. A good agreement in the blood volume measurements, with a very minor bias (~1 mL), can be observed between the two imaging techniques in both the ascending and descending aorta in all subjects.

The linear mixed model analysis led to overall slopes and corresponding confidence intervals of 1.1 ± 0.25 and 0.98 ± 0.08 for the mean velocity in the ascending and descending aorta, respectively, which shows no significant difference between the mean velocity measurements using the standard 2D sequence and the proposed undersampled 3D EPI–CS sequence.

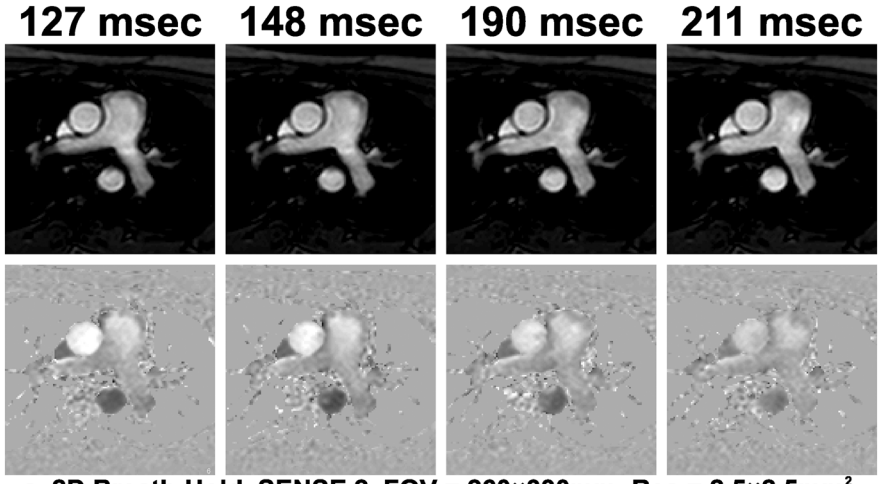

Figure 7. Representative frames of magnitude and flow images acquired using the standard two-dimensional (2D) and the proposed three-dimensional (3D) acquisitions with an echo planar imaging (EPI) factor of 3 and a compressed sensing (CS) rate of 3. The representative slice for the 3D scan was visually selected to match the slice in the 2D scan. As a result of the different temporal resolutions between the two scans (21 ms for the 2D scan and 30 ms for the 3D scan), the time frames cannot be perfectly aligned. Therefore, we chose the closest time frame when needed.

Copyright © 2014 John Wiley & Sons, Ltd.

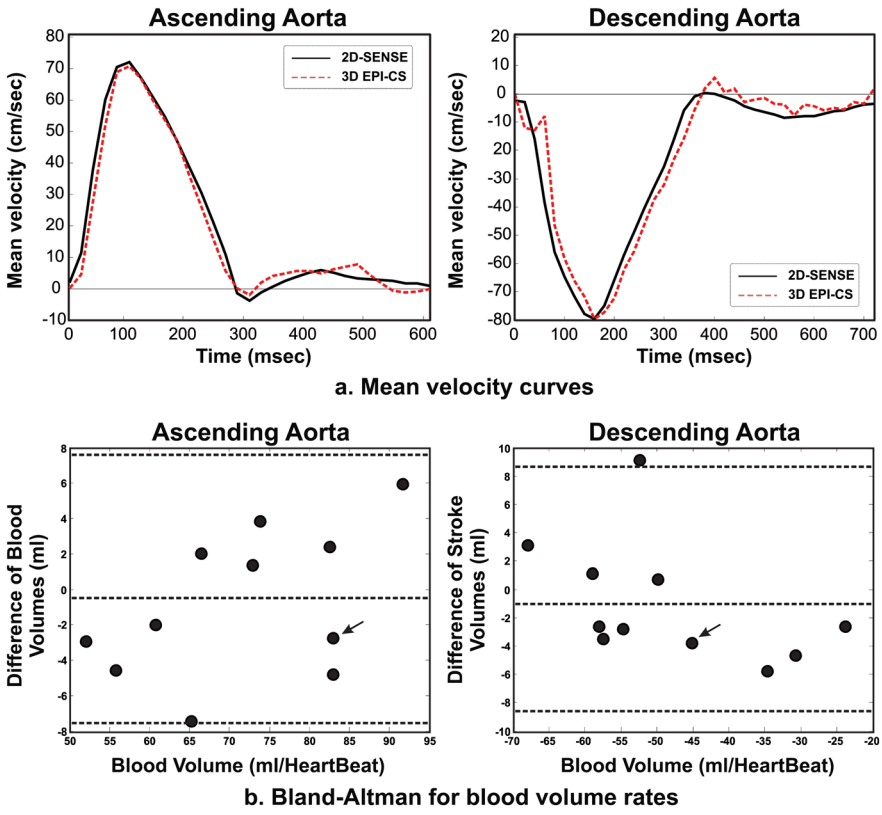

Figure 8. (a) Representative mean ascending and descending aorta velocities from both two-dimensional (2D) and three-dimensional (3D) acquisitions, and using 2D and 3D echo planar imaging–compressed sensing (EPI–CS) sequences. (b) Bland–Altman plots for blood volume rates in both ascending and descending aorta, and measured from 2D and 3D EPI–CS sequences. The arrows point to the subject from which the representative flow curves in (a) are measured. The blood volume rate in the ascending aorta is usually regarded as the stroke volume.

DISCUSSION

We have proposed and demonstrated a 3D EPI–CS cine phase contrast, combining an EPI acquisition with random undersampling of *k* space to reduce the scan time. Using both CS and EPI may be beneficial for 3D cine phase contrast MRI in multiple ways. First, the flow quantification from flow images is based mainly on the phase difference between two phase images, which may remove potential residual artifacts resulting from the CS reconstruction. Second, when EPI is used, it saves the repetition of the relatively long flow encoding gradients which need to be applied after each RF excitation, which, in turn, reduces the TR and thus reduces the scan time.

However, although this combination is promising, it requires special care when designing the corresponding pulse sequence and choosing the acceleration rates, such that the quality of both the flow images and the measurements is not compromised. In this work, we conducted a pilot *in vivo* study to explore the effect of different rates of EPI and CS acceleration on image quality.

Another concern when combining EPI with CS is the effect of the EPI gradient blips. Changing the randomization pattern in between the EPI *k*-space blocks is advantageous as it allows different EPI blocks to be used (i.e. EPI blocks do not need to be replicas of each other). Thus, the center area needs to be fully sampled in the center block only, and not in the other blocks, leading to more efficient sampling. However, this necessitates changing the gradient blips from one profile to another during the acquisition. This usually results in unexpected eddy currents and imbalances in the gradient delay, which, in turn, lead to undesirable artifacts that are difficult to correct using the standard EPI corrections. In this work, we designed the combination of EPI and CS, such that it has constant gradient blips over the whole acquisition to minimize the eddy current artifacts. This implies a constraint on the CS randomization pattern to be exactly the same between the EPI blocks (i.e. all EPI blocks are exact replicas of each other). However, we did not explicitly study the comparison between changing the CS randomization pattern and changing the EPI gradient blips in this work.

Using the proposed sequence, a reduction in scan time of approximately 50% was achieved relative to a standard parallel imaging of rate 4 (i.e. SENSE rate 2 in both k_y and k_z). Similar to ref. (16), we were unable to obtain results of sufficient quality for clinical usage when using SENSE rates above 4 in our pilot study.

The combination of EPI and CS in the proposed sequence was shown to be more advantageous than using each of these methods alone. Recent advances in the hardware side of MR has allowed many technical challenges of EPI acquisitions to be overcome (46). The effect of flow and motion sensitivity on EPI acquisitions has also been well studied (54). However, in our pilot study, using EPI acceleration only failed for EPI rates larger than 5 (i.e. EPI rate of 7 or 9). This was mainly a result of a long TE (TE $>$ 4 ms) which makes the measurements very susceptible to B_0 field inhomogeneity. Moreover, the long TE/TR led to temporal smoothing artifacts, especially in the time phases around the high peak velocities. Recently, CS has been proposed to reduce

Copyright © 2014 John Wiley & Sons, Ltd.

NMR IN BIOMEDICINE

the scan time in flow imaging, and showed good agreement with results from parallel imaging (32). In our pilot study, CS rates of 3 and 4 were achieved with acceptable visual image quality. However, at higher rates (≥5), image quality deteriorated significantly, similar to previous work (34).

In this study, the combination of EPI and CS provided a reasonable TR (~7 ms) and adequate *k*-space coverage. This TR value helps to avoid any excessive field inhomogeneity effect, usually associated with higher EPI rates. Furthermore, the CS rate utilized allows for sufficient *k*-space coverage, enabling a high-quality estimation of the unacquired *k*-space data with the reconstruction algorithm.

Although the undersampling in the proposed sequence resulted in many aliasing and incoherent artifacts in the magnitude (i.e. anatomical) images, our results showed that the flow images, and thus the flow information, were not significantly affected. Visually, the flow results of 3D EPI–CS match well with the corresponding ones of standard 2D phase contrast. Moreover, the flow quantifications show no systematic difference in flow measurements between standard 2D phase contrast and the proposed 3D cine phase contrast MRI with CS and EPI. The main reason is that many of the CS aliasing artifacts, especially those resulting from static tissues, cancel out during the subtraction process used to obtain the flow images, as described in ref. (33).

The LOST algorithm was used in this study for CS reconstruction. A detailed comparison of this method with existing CS methods has been performed elsewhere, where it was shown to improve on existing CS methods in terms of image sharpness for coronary MRI (47). As the specifics of the CS reconstruction were not the focus of this study, this algorithm was not compared with existing CS methods in the context of phase contrast imaging.

In this study, we did not exploit temporal redundancy to enhance the image reconstruction, and possibly to reduce the scan time further. Spatiotemporal *k–t* methods have been shown to increase acceleration rates beyond standard parallel imaging techniques (22–27), albeit at the cost of temporal smoothing in the resulting images. Moreover, flow imaging might be a promising candidate for such techniques, as the spatiotemporal variations in flow images are limited to the blood vessel regions, implying that the image data can be sparsified in an appropriate transform domain, facilitating CS reconstruction. However, a detailed study is needed to carefully address the effect of such reconstruction methods on the accuracy of the flow quantifications through time (22,23), and to study the compromise between such effects and the projected gain in acceleration rate.

In our study, we did not investigate the acceleration that can be achieved with CS alone. Previous studies have investigated the efficacy of CS alone in reducing the scan time for phase contrast MRI (28,30,31,34).

One drawback of the proposed combination of EPI and CS is the lower efficiency of *k*-space coverage. In most 3D acquisitions, the outer region profiles of *k* space (i.e. edges of *k* space) are either heavily undersampled or incompletely acquired [e.g. elliptical shutter strategy (55)]. This usually increases the scan time efficiency by around 10–20%. However, these methods cannot be applied in the proposed sequence because of the inherited features of the EPI acquisition, where each non-acquired profile in the outer region of *k* space leads to non-acquired profiles in the center region, which conflicts with the strategy of fully sampling the center region of *k* space, needed to estimate the coil sensitivity maps and to facilitate CS reconstruction. This leads to inefficiencies in the sampling patterns, as multiple replicas of the fully sampled central blocks are acquired in outer *k* space, and as an elliptical shutter cannot be utilized.

CONCLUSION

An accelerated 3D EPI–CS cine phase contrast sequence, combining an EPI acquisition with random undersampling of *k* space, allows a reduction in scan time by a factor of 7 without compromising the flow quantification measured by standard 2D cine phase contrast MRI.

Acknowledgements

Reconstruction computations of this research were conducted on the Orchestra High Performance Computer Cluster at Harvard Medical School (for more information, see http://rc.hms.harvard.edu).

This work was supported in part by a research grant from Samsung Electronics.

REFERENCES

1. Pelc NJ, Herfkens RJ, Shimakawa A, Enzmann DR. Phase contrast cine magnetic resonance imaging. Magn. Reson. Q. 1991; 7(4): 229–254.
2. Rebergen SA, van der Wall EE, Doornbos J, de Roos A. Magnetic resonance measurement of velocity and flow: technique, validation, and cardiovascular applications. Am. Heart J. 1993; 126(6): 1439–1456.
3. Dumoulin CL, Souza SP, Walker MF, Wagle W. Three-dimensional phase contrast angiography. Magn. Reson. Med. 1989; 9(1): 139–149.
4. Pelc NJ, Bernstein MA, Shimakawa A, Glover GH. Encoding strategies for three-direction phase-contrast MR imaging of flow. J. Magn. Reson. Imaging 1991; 1(4): 405–413.
5. Markl M, Chan FP, Alley MT, Wedding KL, Draney MT, Elkins CJ, Parker DW, Wicker R, Taylor CA, Herfkens RJ, Pelc NJ. Time-resolved three-dimensional phase-contrast MRI. J. Magn. Reson. Imaging 2003; 17(4): 499–506.
6. Gatehouse PD, Keegan J, Crowe LA, Masood S, Mohiaddin RH, Kreitner K-F, Firmin DN. Applications of phase-contrast flow and velocity imaging in cardiovascular MRI. Eur. Radiol. 2005; 15(10): 2172–2184.
7. Lee V, Spritzer C, Carroll B, Pool L, Bernstein M, Heinle S, MacFall J. Flow quantification using fast cine phase-contrast MR imaging, conventional cine phase-contrast MR imaging, and Doppler sonography: in vitro and in vivo validation. Am. J. Roentgenol. 1997; 169(4): 1125–1131.
8. Ebbers T, Wigstrom L, Bolger AF, Wranne B, Karlsson M. Noninvasive measurement of time-varying three-dimensional relative pressure fields within the human heart. J. Biomech. Eng. 2002; 124(3): 288–293.
9. Bley TA, Johnson KM, Francois CJ, Reeder SB, Schiebler ML, Landgraf BR, Consigny D, Grist TM, Wieben O. Noninvasive assessment of transstenotic pressure gradients in porcine renal artery stenoses by using vastly undersampled phase-contrast MR angiography. Radiology 2011; 261(1): 266–273.
10. Markl M, Wallis W, Brendecke S, Simon J, Frydrychowicz A, Harloff A. Estimation of global aortic pulse wave velocity by flow-sensitive 4D MRI. Magn. Reson. Med. 2010; 63(6): 1575–1582.
11. Laffon E, Marthan R, Montaudon M, Latrabe V, Laurent F, Ducassou D. Feasibility of aortic pulse pressure and pressure wave velocity MRI measurement in young adults. J. Magn. Reson. Imaging 2005; 21(1): 53–58.
12. Wentland AL, Wieben O, Francois CJ, Boncyk C, Munoz Del Rio A, Johnson KM, Grist TM, Frydrychowicz A. Aortic pulse wave velocity measurements with undersampled 4D flow-sensitive MRI: comparison with 2D and algorithm determination. J. Magn. Reson. Imaging, 2013; 37(4): 853–859.
13. Dyverfeldt P, Sigfridsson A, Kvitting JP, Ebbers T. Quantification of intravoxel velocity standard deviation and turbulence intensity by generalizing phase-contrast MRI. Magn. Reson. Med. 2006; 56(4): 850–858.
14. Richter Y, Edelman ER. Cardiology is flow. Circulation 2006; 113(23): 2679–2682.

 Copyright © 2014 John Wiley & Sons, Ltd.

15. Bammer R, Hope TA, Aksoy M, Alley MT. Time-resolved 3D quantitative flow MRI of the major intracranial vessels: initial experience and comparative evaluation at 1.5 T and 3.0 T in combination with parallel imaging. Magn. Reson. Med. 2007; 57(1): 127–140.
16. Thunberg P, Karlsson M, Wigström L. Accuracy and reproducibility in phase contrast imaging using SENSE. Magn. Reson. Med. 2003; 50(5): 1061–1068.
17. Peng HH, Bauer S, Huang TY, Chung HW, Hennig J, Jung B, Markl M. Optimized parallel imaging for dynamic PC-MRI with multidirectional velocity encoding. Magn. Reson. Med. 2010; 64(2): 472–480.
18. Thompson RB, McVeigh ER. Flow-gated phase-contrast MRI using radial acquisitions. Magn. Reson. Med. 2004; 52(3): 598–604.
19. Gu T, Korosec FR, Block WF, Fain SB, Turk Q, Lum D, Zhou Y, Grist TM, Haughton V, Mistretta CA. PC VIPR: a high-speed 3D phase-contrast method for flow quantification and high-resolution angiography. Am. J. Neuroradiol. 2005; 26(4): 743–749.
20. Pike GB, Meyer CH, Brosnan TJ, Pelc NJ. Magnetic resonance velocity imaging using a fast spiral phase contrast sequence. Magn. Reson. Med. 1994; 32(4): 476–483.
21. Sigfridsson A, Petersson S, Carlhall CJ, Ebbers T. Four-dimensional flow MRI using spiral acquisition. Magn. Reson. Med. 2012; 68(4): 1065–1073.
22. Baltes C, Kozerke S, Hansen MS, Pruessmann KP, Tsao J, Boesiger P. Accelerating cine phase-contrast flow measurements using k-t BLAST and k-t SENSE. Magn. Reson. Med. 2005; 54(6): 1430–1438.
23. Stadlbauer A, van der Riet W, Crelier G, Salomonowitz E. Accelerated time-resolved three-dimensional MR velocity mapping of blood flow patterns in the aorta using SENSE and k-t BLAST. Eur. J. Radiol. 2010; 75(1): e15–e21.
24. Bauer S, Markl M, Foll D, Russe M, Stankovic Z, Jung B. K-t GRAPPA accelerated phase contrast MRI: improved assessment of blood flow and 3-directional myocardial motion during breath-hold. J. Magn. Reson. Imaging 2013; 38(5): 1054–1062.
25. Schnell S, Markl M, Entezari P, Mahadewia RJ, Semaan E, Stankovic Z, Collins J, Carr J, Jung B. k-t GRAPPA accelerated four-dimensional flow MRI in the aorta: effect on scan time, image quality, and quantification of flow and wall shear stress. Magn. Reson. Med. 2014;72(2):522–33.
26. Giese D, Schaeffter T, Kozerke S. Highly undersampled phase-contrast flow measurements using compartment-based k–t principal component analysis. Magn. Reson. Med. 2013; 69(2): 434–443.
27. Knobloch V, Boesiger P, Kozerke S. Sparsity transform k-t principal component analysis for accelerating cine three-dimensional flow measurements. Magn. Reson. Med. 2013; 70(1): 53–63.
28. Holland DJ, Malioutov DM, Blake A, Sederman AJ, Gladden LF. Reducing data acquisition times in phase-encoded velocity imaging using compressed sensing. J. Magn. Reson. 2010; 203(2): 236–246.
29. Gladden LF, Sederman AJ. Recent advances in flow MRI. J. Magn. Reson. 2013; 229: 2–11.
30. Benning M, Gladden L, Holland D, Schonlieb CB, Valkonen T. Phase reconstruction from velocity-encoded MRI measurements—a survey of sparsity-promoting variational approaches. J. Magn. Reson. 2014; 238: 26–43.
31. Kwak Y, Nam S, Akçakaya M, Basha TA, Goddu B, Manning WJ, Tarokh V, Nezafat R. Accelerated aortic flow assessment with compressed sensing with and without use of the sparsity of the complex difference image. Magn. Reson. Med. 2013; 70(3): 851–858.
32. Kim D, Dyvorne HA, Otazo R, Feng L, Sodickson DK, Lee VS. Accelerated phase-contrast cine MRI using k-t SPARSE-SENSE. Magn. Reson. Med. 2012; 67(4): 1054–1064.
33. Barger AV, Peters DC, Block WF, Vigen KK, Korosec FR, Grist TM, Mistretta CA. Phase-contrast with interleaved undersampled projections. Magn. Reson. Med. 2000; 43(4): 503–509.
34. Tariq U, Hsiao A, Alley M, Zhang T, Lustig M, Vasanawala SS. Venous and arterial flow quantification are equally accurate and precise with parallel imaging compressed sensing 4D phase contrast MRI. J. Magn. Reson. Imaging 2013; 37(6): 1419–1426.
35. Hsiao A, Lustig M, Alley MT, Murphy MJ, Vasanawala SS. Evaluation of valvular insufficiency and shunts with parallel-imaging compressed-sensing 4D phase-contrast MR imaging with stereoscopic 3D velocity-fusion volume-rendered visualization. Radiology 2012; 265(1): 87–95.
36. Hsiao A, Lustig M, Alley MT, Murphy M, Chan FP, Herfkens RJ, Vasanawala SS. Rapid pediatric cardiac assessment of flow and ventricular volume with compressed sensing parallel imaging volumetric cine phase-contrast MRI. Am. J. Roentgenol. 2012; 198(3): W250–W259.
37. Firmin DN, Klipstein RH, Hounsfield GL, Paley MP, Longmore DB. Echo-planar high-resolution flow velocity mapping. Magn. Reson. Med. 1989; 12(3): 316–327.
38. McKinnon GC, Debatin JF, Wetter DR, von Schulthess GK. Interleaved echo planar flow quantitation. Magn. Reson. Med. 1994; 32(2): 263–267.
39. Debatin JF, Leung DA, Wildermuth S, Botnar R, Felblinger J, McKinnon GC. Flow quantitation with echo-planar phase-contrast velocity mapping: in vitro and in vivo evaluation. J. Magn. Reson. Imaging 1995; 5(6): 656–662.
40. Duerk JL, Simonetti OP. Theoretical aspects of motion sensitivity and compensation in echo-planar imaging. J. Magn. Reson. Imaging 1991; 1(6): 643–650.
41. Butts K, Riederer SJ. Analysis of flow effects in echo-planar imaging. J. Magn. Reson. Imaging 1992; 2(3): 285–293.
42. Nishimura DG, Irarrazabal P, Meyer CH. A velocity k-space analysis of flow effects in echo-planar and spiral imaging. Magn. Reson. Med. 1995; 33(4): 549–556.
43. Slavin GS, Riederer SJ. Gradient moment smoothing: a new flow compensation technique for multi-shot echo-planar imaging. Magn. Reson. Med. 1997; 38(3): 368–377.
44. Beck G, Li D, Haacke EM, Noll TG, Schad LR. Reducing oblique flow effects in interleaved EPI with a centric reordering technique. Magn. Reson. Med. 2001; 45(4): 623–629.
45. Thompson RB, McVeigh ER. High temporal resolution phase contrast MRI with multiecho acquisitions. Magn. Reson. Med. 2002; 47(3): 499–512.
46. Hetzer S, Mildner T, Möller HE. A modified EPI sequence for high-resolution imaging at ultra-short echo time. Magn. Reson. Med. 2011; 65(1): 165–175.
47. Akcakaya M, Basha TA, Goddu B, Goepfert LA, Kissinger KV, Tarokh V, Manning WJ, Nezafat R. Low-dimensional-structure self-learning and thresholding: regularization beyond compressed sensing for MRI reconstruction. Magn. Reson. Med. 2011; 66(3): 756–767.
48. Akcakaya M, Basha TA, Chan RH, Rayatzadeh H, Kissinger KV, Goddu B, Goepfert LA, Manning WJ, Nezafat R. Accelerated contrast-enhanced whole-heart coronary MRI using low-dimensional-structure self-learning and thresholding. Magn. Reson. Med. 2012; 67(5): 1434–1443.
49. Wang Y, Riederer SJ, Ehman RL. Respiratory motion of the heart: kinematics and the implications for the spatial resolution in coronary imaging. Magn. Reson. Med. 1995; 33(5): 713–719.
50. Danias PG, Stuber M, Botnar RM, Kissinger KV, Edelman RR, Manning WJ. Relationship between motion of coronary arteries and diaphragm during free breathing: lessons from real-time MR imaging. Am. J. Roentgenol. 1999; 172(4): 1061–1065.
51. Akçakaya M, Basha TA, Chan RH, Manning WJ, Nezafat R. Accelerated isotropic sub-millimeter whole-heart coronary MRI: compressed sensing versus parallel imaging. Magn. Reson. Med. 2014; 71(2): 815–822.
52. Akçakaya M, Rayatzadeh H, Basha TA, Hong SN, Chan RH, Kissinger KV, Hauser TH, Josephson ME, Manning WJ, Nezafat R. Accelerated late gadolinium enhancement cardiac MR imaging with isotropic spatial resolution using compressed sensing: initial experience. Radiology 2012; 264(3): 691–699.
53. Akcakaya M, Basha TA, Chan RH, Rayatzadeh H, Kissinger KV, Goddu B, Goepfert LA, Manning WJ, Nezafat R. Accelerated contrast-enhanced whole-heart coronary MRI using low-dimensional-structure self-learning and thresholding. Magn. Reson. Med. 2012; 67(5): 1434–1443.
54. Luk Pat GT, Meyer CH, Pauly JM, Nishimura DG. Reducing flow artifacts in echo-planar imaging. Magn. Reson. Med. 1997; 37(3): 436–447.
55. Bernstein MA, Fain SB, Riederer SJ. Effect of windowing and zero-filled reconstruction of MRI data on spatial resolution and acquisition strategy. J. Magn. Reson. Imaging 2001; 14(3): 270–280.

Copyright © 2014 John Wiley & Sons, Ltd.